Final Report
USGS NEHRP Grants G11AP20025 G11AP20026
"Delineating future southern Cascadia megathrust rupture with continuous GPS and seismic recordings of Episodic Tremor and Slip (ETS)" with Central Washington University and Miami University

01 Jan. 2011–31 Dec. 2011

Timothy Ian Melbourne

Central Washington University
Ellensburg, WA 98926
(509)-963-2799
tim@geology.cwu.edu

Michael R. Brudzinski

Miami University
Oxford, OH 45056
(513)-529-9758
brudzimr@muohio.edu

Walter Szeliga

Central Washington University
Ellensburg, WA 98926
(509)-963-2705
walter@geology.cwu.edu

Introduction

In recent years, advances in seismic and geodetic monitoring systems have led to the discovery of a unique class of slow earthquakes, which includes extended duration episodes of tectonic tremor and transient slip, occurring inside the transition zone of the subduction interface (e.g. *Beroza and Ide*, 2011). Surface-based geodetic instruments are able to provide clear evidence of recurring episodes of transient slip, showing ground motions opposite of the direction of relative plate convergence, with durations on the order of days to weeks, consistent with the expansion of slow aseismic slip along the subduction interface (*Dragert et al.*, 2001). Often associated with these episodes of transient slip is an emergent, extended duration seismic signal enriched in low-frequency energy referred to as tectonic tremor (*Rogers and Dragert*, 2003). The close spatial and temporal coincidence of tectonic tremor and transient slip, referred to as episodic tremor and slip, observed in several subduction zones suggests these two phenomena are different manifestations of a single source process (*Rogers and Dragert*, 2003; *Obara et al.*, 2004; *Peterson and Christensen*, 2009; *Brudzinski et al.*, 2010).

Preliminary work using a suite of 15 ETS events imaged with GPS and seismic data between 1997–2008 within the Olympic Peninsula region of the northern Cascadia subduction zone shows that the fault is accumulating stress to at least 25 km depth, well inland of the Pacific coast (*Chapman and Melbourne*, 2009). Although delineated using ETS, this plate coupling profile also accurately predicts current, GPS-measured interseismic deformation of the overlying North American plate, as constrained by nearly 100 new continuous GPS receivers. Moreover, when extrapolated over the 550-year average recurrence interval of great Cascadia megathrust earthquakes, the ETS-delineated coupling profile also replicates both the pattern and amplitude of coseismic coastal subsidence inferred for previous great earthquakes (*Chapman and Melbourne*, 2009). Most importantly, this ETS-delineation of seismogenic locking refines previous estimates of megathrust hazards along the Washington State coastal region: it predicts significant coseismic slip nearly 100 km closer to Seattle than the widely-accepted Cascadia rupture paradigm in which coseismic rupture is assumed to stop offshore. Moreover, the ETS-delineated coupling also predicts nearly half of ongoing tectonic convergence, upwards of 9 meters of slip assuming a 550-yr recurrence, will be released beneath the western margin of the greater Seattle-Tacoma metropolitan region at 25 km depth. For the Washington State segment of Cascadia, this translates into a Mw=8.9 source extending near WashingtonÕs metropolitan region. If coupling is similar throughout the arc (which is not known), an Mw=9.2 event is expected for rupture of the entire Cascadia margin.

GPS-determined slip and seismic tremor thus offers a new means of mapping current fault locking and future rupture, magnitude and associated hazards of future earthquakes on the Cascadia megathrust fault. We present preliminary work towards mapping the along-strike variation of seismogenic plate coupling along the southern Cascadia megathrust fault using Episodic Tremor and Slip (ETS).

Tremor Catalog

A catalog of prominent tectonic tremor activity between 2005 and 2011 is constructed by applying a newly designed automated location routine to seismic data spanning the entire length of the Cascadia subduction zone (Figure 1). The framework of the automated tremor location routine is derived from a recently developed semi-automated location routine (*Boyarko and Brudzinski*, 2010), which identifies time periods of elevated levels of tectonic tremor energy utilizing a recently developed tremor detection algorithm (*Brudzinski and Allen*, 2007), identifies the most pronounced signals on stacked envelope seismograms, and inverts analyst refined arrival times for source locations. The automated location routine incorporates two additional components: the definition of evenly spaced networks subsets to aid in detection of concurrent tremor at different locations along strike and a waveform correlation procedure to calculate waveform similarity and perform arrival time refinement. Together, these additional components facilitate a purely objective means of identifying and locating tectonic tremor, although the technique remains biased towards the larger bursts of tremor energy. This procedure is computationally efficient and readily applicable to permanent and temporary seismic networks, allowing us to expand the scope of the previous semi-automated analysis of tectonic tremor both spatially and temporally.

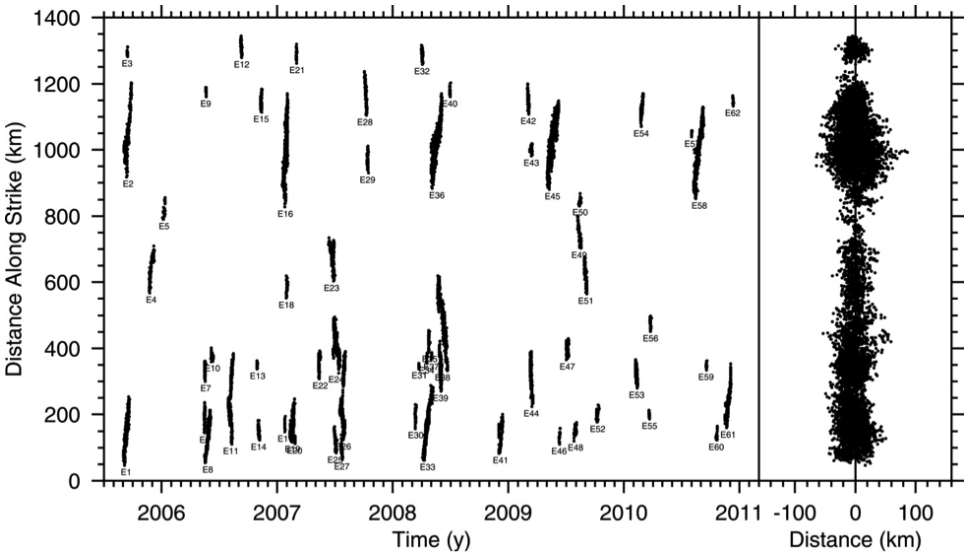

Figure 1: Spatial and temporal distribution of tremor solutions obtained from automated analysis of time periods with increased activity in the tremor passband. In this projection, the distance along strike is measured along the center of the tremor source region. (left panel) Along strike distribution of tremor over time. (right panel) Along strike variations of the strike normal distribution of tremor. For geographical reference, the coastline and political boundaries have been corrected relative to the center of the tremor source region.

Interplate Coupling and Tectonic Tremor

Throughout the Cascadia subduction zone, the tremor source zone exhibits a well-defined updip edge which is distinctly offset from the downdip edge of the geodetically-inferred seismogenic zone (Figure 2). This observation raises some fundamental questions regarding the degree of communication between two zones of capable of generating dynamic instabilities. How exactly is slip accommodated between the downdip edge of the seismogenic transition zone and the tremor and slip source region? How efficiently are stresses transmitted between the episodes of tremor and slip and the seismogenic transition zone? In Cascadia, the absence of historic great earthquakes and extremely low levels of interplate seismicity have inhibited a direct description of the seismogenic zone. Instead, thermal and geodetic estimates of interplate seismogenic potential have served as proxies for characterizing the dimensions of the seismogenic zone. The thermal definition of the seismogenic locked and transition zones correspond with the 100–350°C and 350–450°C interplate temperature ranges (*Hyndman and Wang*, 1995). Geodetic estimates of long-term tidal and leveling records constrain the downdip extent of the seismogenic coupling in southern Cascadia (*Burgette et al.*, 2009), whereas geodetic estimates of continuous GPS time series constrain the downdip extent of the seismogenic coupling in northern Cascadia (*McCaffery*, 2009). The average distance between the downdip edge of the seismogenic zone and the tremor source region varies along strike (Figure 2). The downdip edge of the geodetic seismogenic zone abuts the tremor source zone in southern Cascadia but is offset by as much as 50 km in the northern half of the subduction zone.

It is important to underscore that in subduction zones where tectonic tremor and transient slip are both present, there tends to be a gradation in the style of deformation with depth on the plate interface. Specifically, the peak in the distribution of transient slip is typically offset updip from the peak in the distribution of tectonic tremor, filling the gap between the seismogenic zone and the tremor source region (*Wang et al.*, 2008; *Song and Simons*, 2003; *Wech et al.*, 2009; *McCaffery*, 2009; *Brudzinski et al.*, 2010). The implications of this relationship are most profound in regions where the geodetic transition zone abuts or overlaps the tremor zone is where one might expect the probability of static or dynamic stresses during either seismogenic or transient deformation episodes to be greatest. Positive changes in static stress resulting from transient slip are modeled to bring the locked zone closer to failure (*Dragert et al.*, 2004). As well, slow dynamic instabilities via transient slip could conceivably continue to propagate updip and evolve into an earthquake triggering mechanism. Moreover, dynamic instabilities via megathrust earthquakes could continue to propagate down-dip into the tremor and slip zone. This implies that coseismic slip may be accommodated as much as 50-100 km further inland than was previously thought. However, the complex spatial relationships between the locked zone, slow slip and tremor suggest that potential triggering relationships are not straightforward.

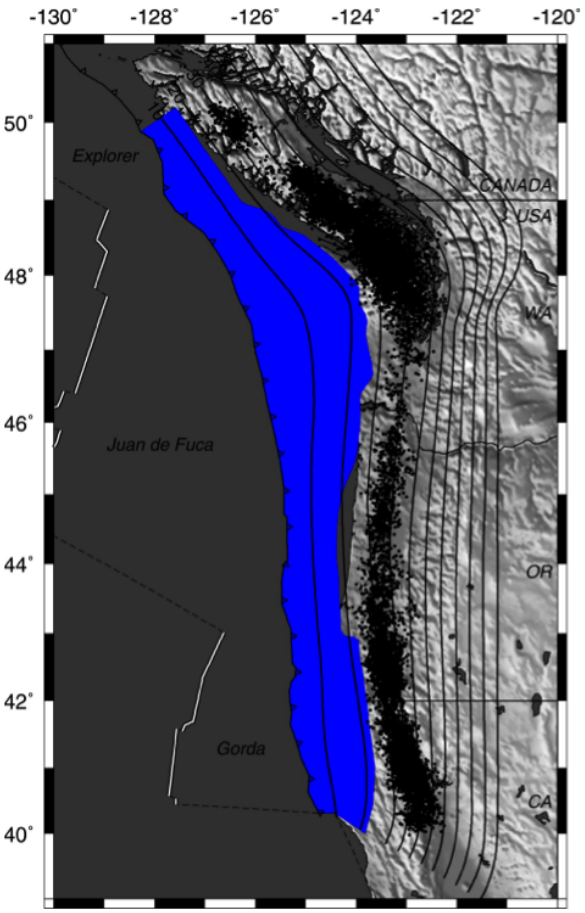

Figure 2: Map of tectonic tremor and interpretation of the seismogenic portion of the subduction interface inferred from estimates of interseismic coupling (*McCaffery*, 2009; *Burgette et al.*, 2009).

Geodetic Catalog

We have utilized the plethora of GPS station available to us in southern Cascadia to extend the mapping of Episodic Tremor and Slip (ETS) slip patches south of latitude 45°N. ETS slip patches have been shown to delineate the down-dip limit of plate coupling and thus, the maximum down-dip width of coseismic rupture during a megathrust earthquake (*Chapman and Melbourne*, 2009). Since the completion of the Plate Boundary Observatory (PBO), the increase in the spatial density of the GPS network along the southern Cascadia margin now allows us to geodetically resolve ETS events south of latitude $\approx 45°$N and estimate the maximum size and region of influence of megathrust earthquakes, in southern Cascadia.

Previous work has focused primarily on delineating the maximum down-dip rupture extent in the Puget Sound area (*Chapman and Melbourne*, 2009). This focus on the Puget Sound region was primarily due to the shear spatial density of the GPS network relative to regions farther south along the Cascadia margin. However, with the recent completion of the PBO GPS network, the region south of the Puget Sound, through coastal Oregon and northern California, has greatly increased the theoretical slip resolution (Figure 3).

In this study, we have focused primarily on ETS events recorded south of a latitude of 45°N during the time period 2008–2012. During this period, nine distinct ETS events were observed geodetically (Figure 4). The first ETS event in this period began in Mar. of 2008 and shows deformation on stations at the extreme southern end of the network at $\approx 40°$N. The next ETS event in this period began in May of 2008 and shows deformation on stations northward to nearly $\approx 45°$N. The final ETS event of 2008 shows deformation, again on stations at the extreme southern end of the network.

During 2009, there were two ETS events. The first ETS event of 2009 began in March with deformation appearing primarily on stations south of $\approx 43°$N. Following the March 2009 ETS event, offsets from an apparently smaller ETS event appear on GPS stations near $\approx 43°$N, however deformation was only observed on 2 GPS stations. Another ETS event appears during Jul. of 2009 at the extreme southern end of the network and scattered offsets appear north of $\approx 43°$N for the remainder of 2009 and beginning of Jan. 2010, when offsets were observed across the majority of the plate interface between $41.5°$N and$45°$N .

ETS activity began again in Feb. 2010 with offsets observed along the California-Oregon border. Later during 2010, there were two ETS events observed across the extreme southern end of the network; one in Mar. and one that lasted from Sep. until Oct. The final temporal cluster of offsets for the period under examination occurs in January 2011 around the latitude of $\approx 43°$N. Sporadic or poorly recorded offsets are seen near May 2011 along the southern segment of the network, but, due to the small number of stations involved, meaningful data inversions were not possible.

Methods

We proceed using similar methods to *Szeliga et al.* (2008), by examining record sections of the margin perpendicular component of GPS station position time series. For the

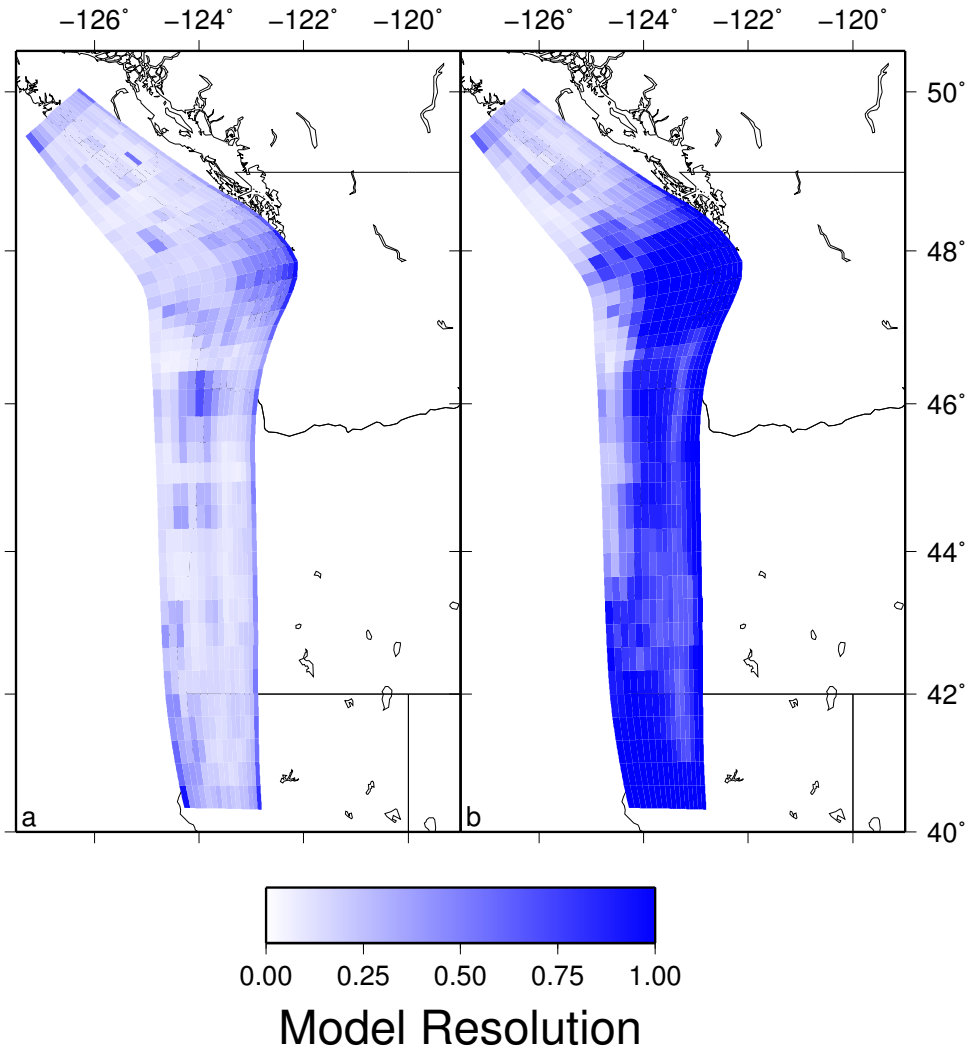

Figure 3: Theoretical model resolution for the pre-PBO and post-PBO station geometries. A value of 1 indicates regions where the true slip value could be recovered in an inverse problem, while a value of 0 indicates region where no slip is theoretically recoverable in an inverse problem. a.) pre-PBO GPS station geometry b.) post-PBO GPS station geometry.

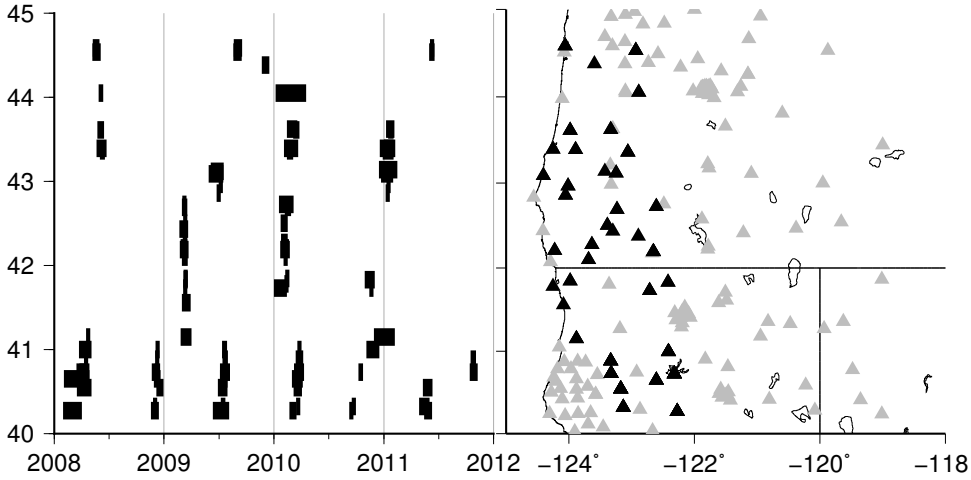

Figure 4: Timing of slow earthquake signals along the southern Cascadia margin plotted by station latitude. Black triangles indicate GPS stations that display slow earthquake offsets during the period 2008–2012. Gray triangles show the extent of the PBO network in southern Cascadia.

southern segment of the Cascadia subduction zone, we focus our initial attention on the longitude component due to the primarily northerly strike of the subducting plate south of $\approx 46°$. We create record sections from the longitude component of the GPS time series and order them by latitude to facilitate the identification of spatial continuity as well as temporal continuity in any transient signal. At this stage, we focus on identifying the approximate times of initiation for possible ETS offsets. Once a preliminary catalog of rough ETS initiation times has been created, we proceed by refining these times and estimate duration, offset magnitude and uncertainty.

We experimented with a new approach to estimating onset, duration, offset and uncertainty by using a Markov Chain Monte Carlo method (*Mosegaard and Tarantola*, 1995). This approach consisted of exploring the model space using an equation of the form,

$$y = a + bt + \sum_{i=1}^{n} \frac{U_i}{2}\left[\tanh\left(\frac{(x - T_i)}{\tau_i}\right) - 1.0\right]$$

where a is the y-intercept, b is the secular rate, t is time, U_i, T_i, and τ_i are the displacement, mid-point time, and duration of the ith ETS event respectively (*Larson et al.*, 2004). However, the quality of our results varied significantly, primarily depending on the noise spectrum of the time series, and this approach was only successful in estimating 14 of the 48 offsets identified. For estimating the parameters of the remaining offsets, we utilize the approach taken in *Szeliga et al.* (2008).

Once our refined catalog of ETS offsets was assembled, we inverted for slip on the plate interface, using plate model from (*Flück et al.*, 1997) with a fault spacing of ≈ 25 km $\times$ 15 km and the non-negative least squares methodology outlined in (*Szeliga*

et al., 2008).

Results

Episode	Year-Month	Region	M_w (mm)	Peak slip
G1	2008-Mar.	south	6.4	36
G2	2008-May	central	6.7	24
G3	2008-Nov.–Dec.	south	6.8	33
G4	2009-Mar.	central	6.7	27
G5	2009-Jul.	south	6.4	35
G6	2010-Feb.	central	6.6	25
G7	2010-Mar.	south	6.4	28
G8	2010-Sep.–Oct.	south	6.7	26
G9	2011-Jan.	central	6.8	32

Table 1: Equivalent magnitude and peak slip for ETS events in south and south-central Cascadia.

For the following figures, in order to identify and highlight artifacts due to station geometry in our inversion, we have taken the inverted slip distribution and then altered the color saturation of each fault patch according the the theoretical model resolution (*Menke*, 1989). Theoretical model resolution depends entirely on the geometry of the GPS network and the geometry of the fault, and can be calculated in the absence of offset data. In the figures, fault patches with poor model resolution are desaturated, i.e. shifted towards white. This allows the eye to more easily ignore spurious slip patches in regions of poor model resolution that arise from the spatial smoothing imposed to regularize the inverse problem. Depth contours in our fault model are 2.5 km, with the shallowest fault edge at a depth of 10 km. This coarse depth spacing, combined with the often small geodetic signal size and the attenuating effects of the elastic crust, are the primary limits on the precision of our rupture limit estimates.

Figure 5 shows the results of the inversion of the GPS offsets from the 2008 ETS events. Slip during both the Mar. and Nov.–Dec. 2008 ETS events appear to concentrate along the southern boundary of the fault model, consistent with the offsets appearing primarily on southerly GPS stations. Slip appears across a wide range of depths, between depths of 22.5 km and 37.5 km during the Mar. 2008 ETS and between 30 km and 47.5 km during the Nov.–Dec. 2008 ETS event. This may reflect the interplay between the regularization boundary condition at the southern edge of the fault model. Slip during the May 2008 ETS event appears to be separated into two distinct lobes, and may be continuous with a central Cascadia (north of $45°$N) ETS event during the same time period. Peak slip, constrained to lie on the plate interface is 2.4 cm, with a total moment release equivalent to Mw 6.7. The maximum down-dip rupture limit that

may be confidently assigned is approximately 17.5 km depth, but possibly as shallow as 15 km depth at a latitude of 44°N and 17.5 km at 45.5°N.

Slip during the March 2009 ETS event (Figure 6) was primarily located between 42°N and 43°N, with a peak slip of 2.7 cm and a total moment release equivalent to Mw 6.7. The maximum down-dip rupture limit estimate from this slip patch is approximately 20 km depth at 42.5°N. Similar to the southernmost ETS events in 2008, the Jul. 2009 ETS event displays slip across a range of depths, with sizable slip down to 42.5 km.

Slip during the Feb. 2010 ETS event (Figure 7) was located in two patches, one SW-NE swath at 42°N and a slightly larger patch near 44°N. Peak slip was 2.5 cm with an equivalent moment magnitude of Mw 6.6. The maximum down-dip rupture limit estimate from this slip patch is approximately 20 km depth at 42°N and 25 km depth near 44°N. Slip along the southernmost ETS patches is again, distributed across a range of depths. During the Mar. 2010 ETS event, there are hints of a slip patch oriented NW and up-dip of the largest offsets and may represent the northward migration of offsets with time shown in Figure 4. The Sep.–Oct. 2010 ETS event shows a lower amplitude slip patch north of 42°N and may represent slip occuring with northward migration(Figure 4). The temporal continuity of this ETS event sparser than others and the exact behavior of this ETS event isn't clear from geodetic data alone.

Slip during the Jan. 2011 ETS event was located primarily in one large patch near 42°N with lesser amounts of slip north towards 43.5°N. Peak slip was 3.2 cm with an equivalent moment magnitude of Mw 6.8. The maximum down-dip rupture limit estimate from this slip patch is shallower than that estimated from the 2010 ETS event and may be as shallow as 15 km depth at 42°N.

Summing the slip distributions from the ETS events shown in Table 1 during the period 2008–2012 (Figure 9) yields a peak total slip of 16.4 cm and an equivalent total moment release of Mw 7.3. Spatial smearing due to the boundary conditions imposed by the fault shape appear to be responsible for the up-dip smearing of total slip along the southernmost edge of the fault. Consequently, the estimates of the up-dip limit of ETS slip at the southernmost extreme of the Juan de Fuca are less precise. Starting at $\approx$ 41°N, the up-dip limit of ETS slip appears quite shallow, $\approx$ 15km. Farther northward, the up-dip limit appears to become deeper with ETS slip primarily below 22.5 km.

Synthesis

Table 2 shows the synthesis of the tremor catalog and geodetic ETS catalog for data from the southern portion of Cascadia. Tremor episode numbers are derived from the margin-wide catalog shown in Figure 1, while geodetic episode numbers are from Table 1.

While some tremor episodes show a direct overlap geodetic ETS episodes, the correspondence is not always obvious. For example, geodetic episode G5, which began in Jul. 2009 may be correlated with either tremor episode E46, via geodetic onset miscalculation, or E48, or, perhaps, both. The larger pattern that emerges however, is that tremor episodes with rupture lengths greater than $\approx$ 100km show unequivocal

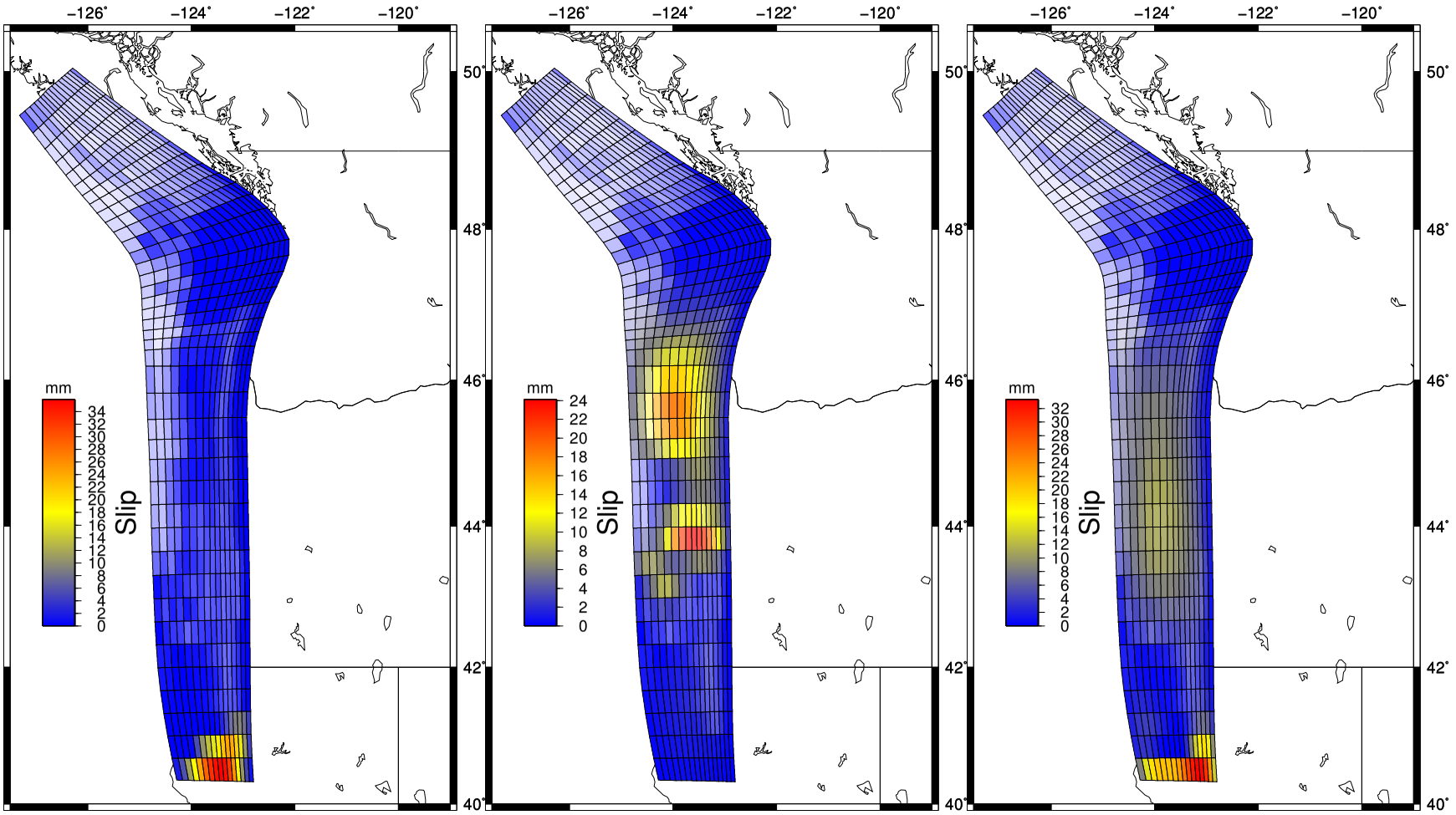

(a) 2008 Mar. (b) 2008 May (c) 2008 Nov.–Dec.

Figure 5: 2008 slip inversions, total magnitude Mw 7.0, total peak slip 6.5 cm

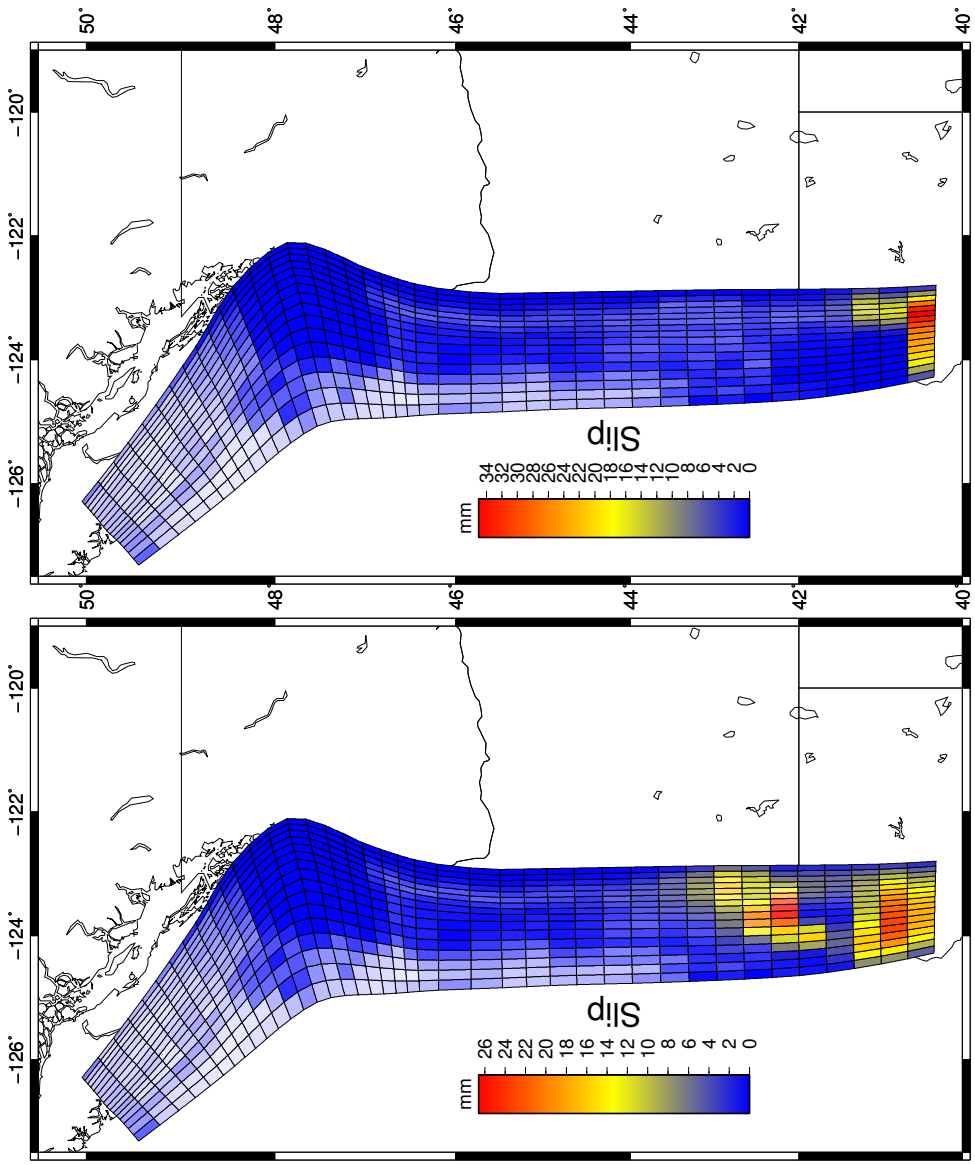

(a) 2009 Mar. (b) 2009 Jul.

Figure 6: 2009 slip inversions, total magnitude Mw 6.8 total peak slip 4.8 cm

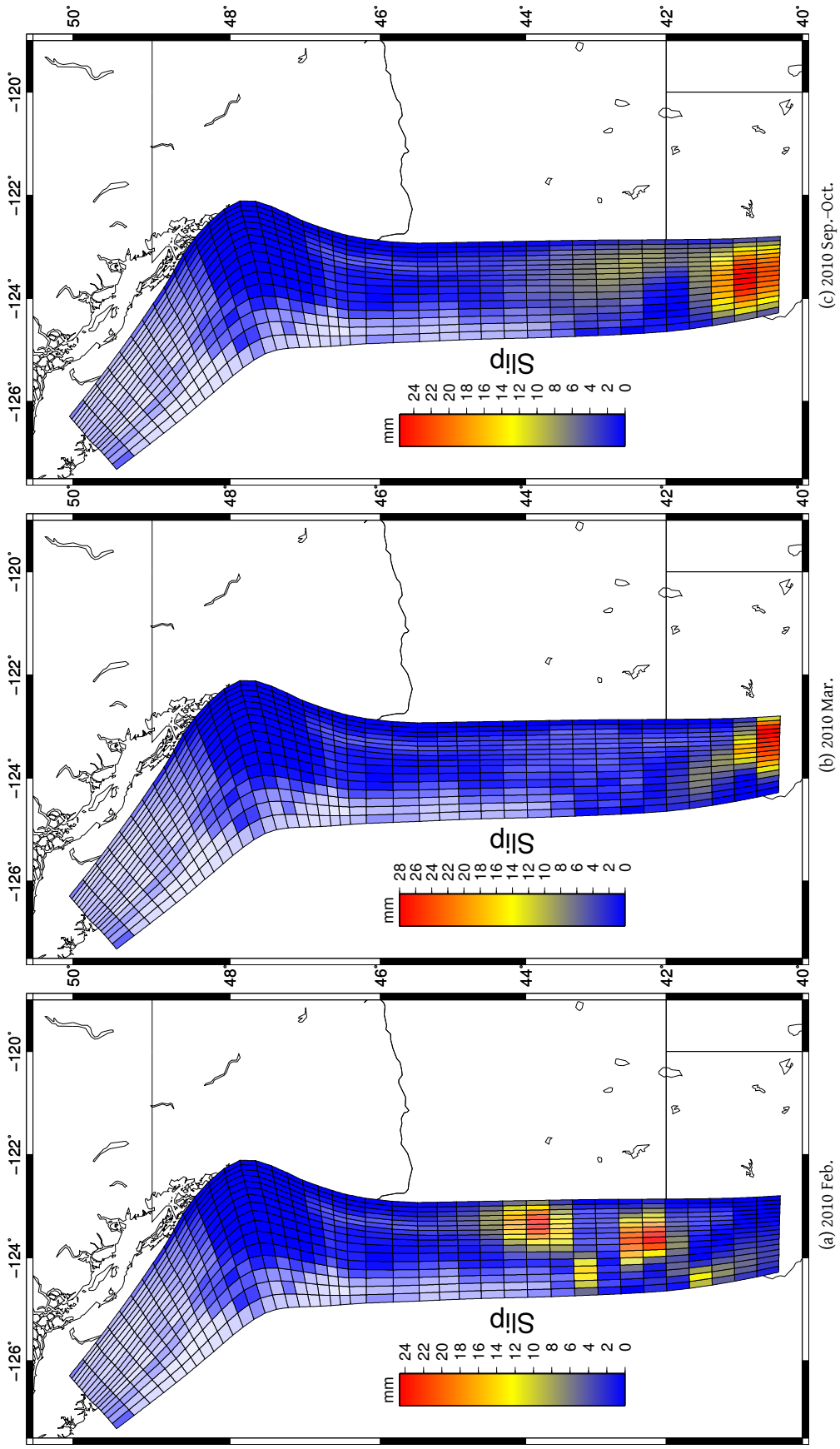

Figure 7: 2010 slip inversions, total magnitude 6.9 Mw, total peak slip 4.7 cm

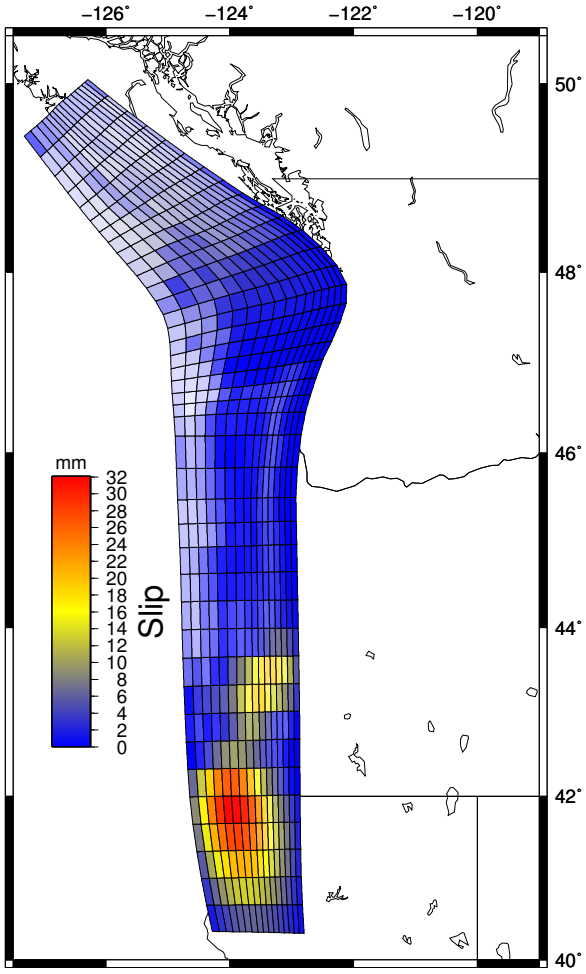

Figure 8: 2011 slip inversion magnitude Mw 6.8 Peak slip 3.2 cm

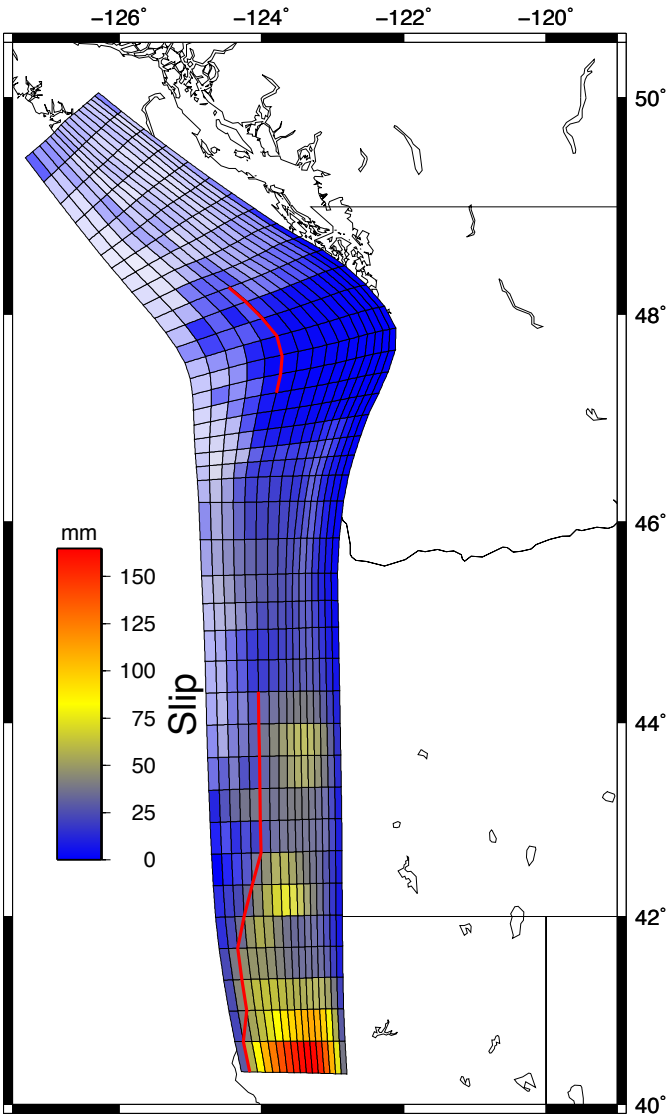

Figure 9: Total slip on the plate interface south of latitude 44°N between 2008–2012. Southernmost red line indicates the inferred down-dip rupture boundary, northern red line is from *Chapman and Melbourne* (2009).

Tremor Episode[a]	Geodetic Episode[b]	Start Date (mm/dd/yyyy)	Duration (days)	Length (km)
E33	G1	03/30/2008	34	220
E38	G2	05/20/2008	33	280
E41	G3	11/30/2008	14	108
E44	G4	03/10/2009	9	156
E46	G5	06/08/2009	5	36
E48		07/25/2009	10	42
E53	G6	02/05/2010	9	78
E55	G7	03/20/2010	3	20
E60	G8	10/17/2010	6	38
E61		11/15/2010	21	180

Table 2: Tremor start dates, durations and rupture lengths for ETS events in south and south-central Cascadia. Values are taken from a larger catalog of margin-wide tremor in (*Boyarko et al., in prep.*). [a] Episode numbers refer to Figure 1. [b] Geodetic episodes defined in Table 1.

geodetic offsets. This is expected, since the station spacing of the network is large, and therefore expected to be most sensitive to large rupture lengths. The relationship between duration and rupture length appears more complicated, and would require a thorough analysis of a larger ETS data set. One final comparison that is worth making is to plot GPS-inferred moment versus tremor duration (Figure 10).

Previous studies (*Aguiar et al.*, 2009) have found a linear relationship between hours of tremor and moment. This behavior is in contrast to the relationship of moment with the cube of duration typical for non-slow earthquakes (*Ide et al.*, 2007). The wide scatter of the southern Cascadia ETS events about the previously inferred moment-hour relationship from *Aguiar et al.* (2009) could possibly arise from the conversion of catalog tremor duration to equivalent tremor hours. Another possibility is a potential bias in the moment calculation for the ETS events along the southernmost edge of the Juan de Fuca due to edge effects in the fault model.

References

Aguiar, A. C., T. Melbourne, and C. W. Scrivner (2009), Moment release rate of Cascadia tremor constrained by GPS, *J. Geophys. Res.*, *114*, B00A05.

Beroza, G. C., and S. Ide (2011), Slow earthquakes and nonvolcanic tremor, *Ann. Rev. Earth Planet. Sci.*, *39*, 271–296, doi:10.1146/annurev-earth-040809-152531.

Boyarko, D. C., and M. R. Brudzinski (2010), Spatial and temporal patterns of non-volcanic tremor along the southern cascadia subduction zone, *J. Geophys. Res.*, *115*, B00A22, doi:10.1029/2008JB006064.

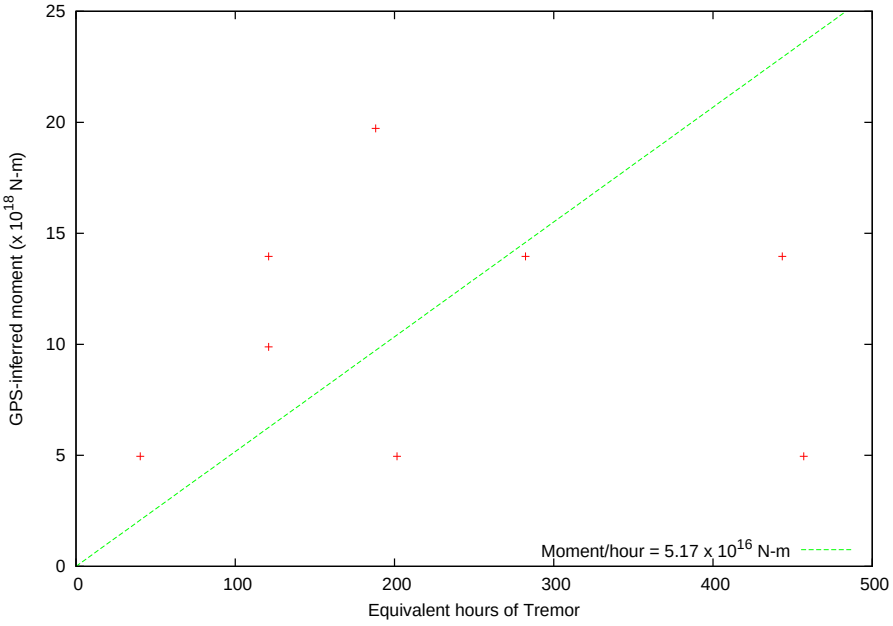

Figure 10: GPS-inferred moment versus equivalent tremor duration. Equivalent tremor duration was calculated from the catalog duration by assuming that tremor was recorded for 56% of each day. The moment-hour relationship is shown for comparison and is from *Aguiar et al.* (2009).

Brudzinski, M. R., and R. M. Allen (2007), Segmentation in episodic tremor and slip all along Cascadia, *Geology*, *35*(10), 907–910.

Brudzinski, M. R., H. R. Hinojosa-Prieto, K. M. Schlanser, E. Cabral-Cano, A. Arciniega-Ceballos, O. Diaz-Molina, and C. DeMets (2010), Nonvolcanic tremor along the Oaxaca segment of the Middle America subduction zone, *J. Geophys. Res.*, *115*, doi: 10.1029/2008JB006061.

Burgette, R. J., R. J. Weldon, and D. A. Schmidt (2009), Interseismic uplift rates for western oregon and along-strike variation in locking on the cascadia subduction zone, *J. Geophys. Res.*, *114*, B01408, doi:10.1029/2008JB005679.

Chapman, J. S., and T. I. Melbourne (2009), Future Cascadia megathrust rupture delineated by episodic tremor and slip, *Geophys. Res. Lett.*, *36*, L22301.

Dragert, H., K. Wang, and T. S. James (2001), A silent slip event on the deeper Cascadia subduction interface, *Science*, *292*, 1525–1528.

Dragert, H., K. Wang, and G. Rogers (2004), Geodetic and seismic signatures of episodic tremor and slip in the northern Cascadia subduction zone, *Earth Planets Space*, *56*, 1143–1150.

Flück, P., R. D. Hyndman, and K. Wang (1997), Three-dimensional dislocation model for great earthquakes of the Cascadia subduction zone, *J. Geophys. Res.*, *102*(9), 20,539–20,550.

Hyndman, R. D., and K. Wang (1995), The rupture zone of Cascadia great earthquakes from current deformation and the thermal regime, *J. Geophys. Res.*, *100*(11), 22,133–22,154.

Ide, S., G. C. Beroza, D. R. Shelly, and T. Uchide (2007), A scaling law for slow earthquakes, *Nature*, *447*, 76–79.

Larson, K. M., A. R. Lowry, V. Kostoglodov, W. Hutton, O. Sánchez, and G. Suárez (2004), Crustal deformation measurements in Guerrero, Mexico, *J. Geophys. Res.*, *109*, B04409.

McCaffery, R. (2009), Time-dependent inversion of three-component continuous GPS for steady and transient sources in northern Cascadia, *Geophys. Res. Lett.*, *36*, L07304, doi:10.1029/2008GL036784.

Menke, W. (1989), *Geophysical data analysis: discrete inverse theory*, Academic Press.

Mosegaard, K., and A. Tarantola (1995), Monte Carlo sampling of solutions to inverse problems, *J. Geophys. Res.*, *100*(7), 12,431–12,447.

Obara, K., H. Hirose, F. Yamamizu, and K. Kasahara (2004), Episodic slow slip events accompanied by non-volcanic tremors in southwest Japan subduction zone, *Geophys. Res. Lett.*, *31*, L23602.

Peterson, C. L., and D. H. Christensen (2009), Possible relationship between nonvolcanic tremor and the 1998–2001 slow slip event, south central Alaska, *J. Geophys. Res.*, *114*, B06302, doi:10.1029/2008JB006096.

Rogers, G., and H. Dragert (2003), Episodic tremor and slip on the Cascadia subduction zone: The chatter of slient slip, *Science*, *300*, 1942–1943.

Song, A. T.-R., and M. Simons (2003), Large trench-parallel gravity variations predict seismogenic behavior in subduction zones, *Science*, *301*, 630–633.

Szeliga, W., T. Melbourne, V. M. Santillan, and M. Miller (2008), GPS constraints on 34 slow slip events within the Cascadia subduction zone, 1997–2005, *J. Geophys. Res.*, *113*, B04404.

Wang, K., H. Dragert, H. Kao, and E. Roeloffs (2008), Characterizing an "uncharacteristic" ETS event in northern Cascadia, *Geophys. Res. Lett.*, *35*, L15303.

Wech, A. G., K. C. Creager, and T. Melbourne (2009), Seismic and geodetic constraints on cascadia slow slip, *J. Geophys. Res.*, *114*, B10316, doi:10.1029/2008JB006090.